© 2016. Published by The Company of Biologists Ltd | Development (2016) 143, 3549-3559 doi:10.1242/dev.137067

RESEARCH ARTICLE

Early formation of the Müllerian duct is regulated by sequential actions of BMP/Pax2 and FGF/Lim1 signaling

Yuji Atsuta[1,*] and Yoshiko Takahashi[1,2,‡]

ABSTRACT

The Müllerian duct (MD) and Wolffian duct (WD) are embryonic tubular tissues giving rise to female and male reproductive tracts, respectively. In amniote embryos, both MD and WD emerge in both sexes, but subsequently degenerate in the males and females, respectively. Here, by using MD-specific gene manipulations in chicken embryos, we identify the molecular and cellular mechanisms that link early MD specification to tubular invagination. Early (pre-) specification of MD precursors in the coelomic epithelium requires BMP signaling and its downstream target Pax2 in a WD-independent process. Subsequently, the BMP/Pax2 axis induces Lim1 expression, a hallmark of MD specification, for which FGF/ERK and WD-derived signals are also required. Finally, the sequential actions of the BMP/Pax2 and FGF/Lim1 axes culminate in epithelial invagination to form a tubular structure driven by an apical constriction, where apical accumulation of phospho-myosin light chain is positively regulated by FGF/ERK signaling. Our study delineates mechanisms governing the early formation of the MD, and also serves as a model of how an epithelial cell sheet is transformed to a tubular structure, a process seen in a variety of developmental contexts.

KEY WORDS: Müllerian duct, Cell specification, Invagination, Apical constriction, Wolffian duct

INTRODUCTION

The male and female reproductive tracts have profoundly different shapes and functions. Despite this profound sexual dimorphism in adults, the embryonic development of the reproductive tract is initiated similarly in both sexes. For example, the Müllerian duct (MD), which gives rise to the oviduct, uterus, cervix and upper part of the vagina, is formed in both female and male, but degenerates in males through the action of anti-Müllerian hormone (also called Müllerian inhibiting substance) produced by the embryonic testes (Behringer et al., 1994). Likewise, the Wolffian duct (WD: also called the nephric duct) contributing to the formation of the epididymis, vas deferens and seminal vesicle in males, emerges in early embryos of both sexes but degenerates afterwards in female embryos (Cunha, 1975; Guioli et al., 2007; Jacob et al., 1999; Mullen and Behringer, 2014). In addition, WD and MD form in close proximity, suggesting the possibility of reciprocal interactions.

In humans, approximately 3% of births are accompanied by female reproductive tract-related disorders, including the Müllerian aplasia, a congenital loss of the uterus and vagina (Ayers et al., 2015; Kobayashi and Behringer, 2003; Layman, 2013; Sandbacka et al., 2013). To understand how these disorders arise, it is important to delineate the mechanisms of MD formation.

During embryonic development in both sexes, the MD arises from the lateral plate-derived coelomic epithelium (CE). The processes of MD development can be divided into distinct phases: initiation, invagination and extension (Orvis and Behringer, 2007). At the initiation phase, cells in the CE juxtaposed to the WD are specified to the MD fate. The specified cells are marked by a placode-like thickening and the expression of the LIM-class homeobox gene *Lim1* (also known as *Lhx1*) (Guioli et al., 2007; Jacob et al., 1999; Kobayashi et al., 2004). In the subsequent phase, cells undergo a dynamic morphogenetic change, invaginating inwards into the mesonephros territory, to form the prospective opening of the MD at the most anterior end (the level of 12th to 15th somites in chickens) (Jacob et al., 1999; Orvis and Behringer, 2007). Following the invagination, the tip of the MD contacts the WD, and extends caudally until it reaches the urogenital sinus. For this extension process, the WD is required (Gruenwald, 1941; Kobayashi et al., 2005; Orvis and Behringer, 2007). Finally, the extended MD gives rise to several distinct reproductive organs in female.

Mouse genetic studies have shown that several transcriptional factors, including Pax2, Pax8 and Lim1 are required for MD development, although how these factors regulate the cellular behavior of the forming MD is not fully understood. Wnt4 and Wnt9b signals have been shown to be important for the extension of the MD rudiment (Bouchard et al., 2002; Carroll et al., 2005; Kobayashi et al., 2004; Prunskaite-Hyyrylainen et al., 2016; Torres et al., 1995; Vainio et al., 1999). However, the mechanisms underlying the initiation phase of MD development remain unknown. In the present study, we examined how the early MD is specified at the molecular and cellular levels using chicken embryos, in which the MD develops similarly to mammals (Guioli et al., 2007; Jacob et al., 1999). Using the chicken *in ovo* electroporation technique (Momose et al., 1999), which allows MD-specific gene manipulations (Ayers et al., 2015; Guioli et al., 2007), we demonstrate that early MD morphogenesis is controlled by multiple morphogenetic factors, including bone morphogenetic protein (BMP), fibroblast growth factor (FGF), and their respective downstream targets Pax2 and Lim1 in harmony with a WD-derived factor. The BMP/Pax2 and FGF/Lim1 axes culminate in invagination of the MD, where apical constriction of the epithelial cell sheet is triggered by FGF/ERK (extracellular signal-related kinase; also known as MAP kinase, MAPK)-mediated phosphorylation of myosin light chains (pMLC).

[1]Department of Zoology, Graduate School of Science, Kyoto University, Kitashirakawa, Sakyo-ku, Kyoto 606-8502, Japan. [2]AMED Core Research for Evolutional Science and Technology (AMED-CREST), Japan Agency for Medical Research and Development (AMED), Chiyoda-ku, Tokyo 100-0004, Japan. *Present address: Department of Genetics, Harvard Medical School, Boston, MA 02115, USA.

‡Author for correspondence (yotayota@develop.zool.kyoto-u.ac.jp)

Y.A., 0000-0002-5116-0800; Y.T., 0000-0002-1596-7527

Received 14 March 2016; Accepted 4 August 2016

Development (2016) 143, 3549-3559 doi:10.1242/dev.137067

RESULTS

Expression of Pax2, Lim1 and N-cadherin during MD specification

Although previous morphological studies reported that MD invagination occurs at Hamburger and Hamilton stage (HH) 24 in chick embryos (Jacob et al., 1999; Guioli et al., 2007), the precise timing of MD specification and the onset of MD invagination have not been documented. To describe molecular and cellular events during early MD development, we examined expression patterns of Pax2, Lim1 and N-cadherin (also known as cadherin 2) in the CE adjacent to the WD, the region known to form MD, in HH16-24 embryos. We excluded Pax8, an early MD marker observed in mice because avian species lost the *Pax8* gene during their evolution (Freter et al., 2012). As shown in Fig. 1, Pax2 starts to be expressed at HH16, and most CE cells become Pax2 positive by HH19 (Fig. 1A-D‴).

At HH21, the Lim1 protein was detected in several cells within the Pax2-positive territory in the CE (Fig. 1E-F‴), and this expression became prominent by HH24 (Fig. 1E-J‴). Almost all the Lim1-positive cells were also Pax2-positive (337 Pax2-positive cells out of 340 Lim1-positive cells in 14 HH23 embryos). Concomitantly with the increase in Lim1 signal, epithelial thickening and subsequent invagination of MD were observed in HH23-24 embryos (Fig. 1G-J‴). We further found apically localized N-cadherin in CE cells at HH23 prior to MD invagination, implying that the apical constriction might trigger the invagination processes (Fig. 1H-H‴).

We noticed that the Lim1-positive domain in the CE was confined within a range measuring 100 µm laterally from the medial edge of the WD (Fig. S1). Because these Lim1-positive CE cells appeared to be MD precursors, this Lim1-positive area was defined as the MD-forming region (MFR). To gain a quantitative understanding of the progressive specification of the MD, the number of Pax2- or Lim1-positive nuclei in the MFR was counted (Fig. S1; Fig. 1K). At HH21, whereas ∼90% of the cells in the MFR expressed Pax2, only a few cells were positive for Lim1, which later increased to ∼75% at HH24 (Fig. 1K). These results suggest that Pax2 and Lim1 act in the CE/MFR at different time points, and also that the expression of these genes are regulated differently.

BMP signals are essential for MD specification by regulating Pax2 expression

Previous studies reported that Lim1 acts downstream of Pax2 in several developmental contexts, including the development of mouse pronephros (Boualia et al., 2013; Bouchard et al., 2002). We therefore investigated whether Pax2 expression in the MFR was required for the expression of Lim1 during MD development. To this end, we used the *in ovo* electroporation technique to introduce *Pax2* shRNA-encoding plasmids into the CE/MFR (Guioli et al., 2007; Watanabe et al., 2007) (Fig. S2; Fig. 1L-P). This treatment

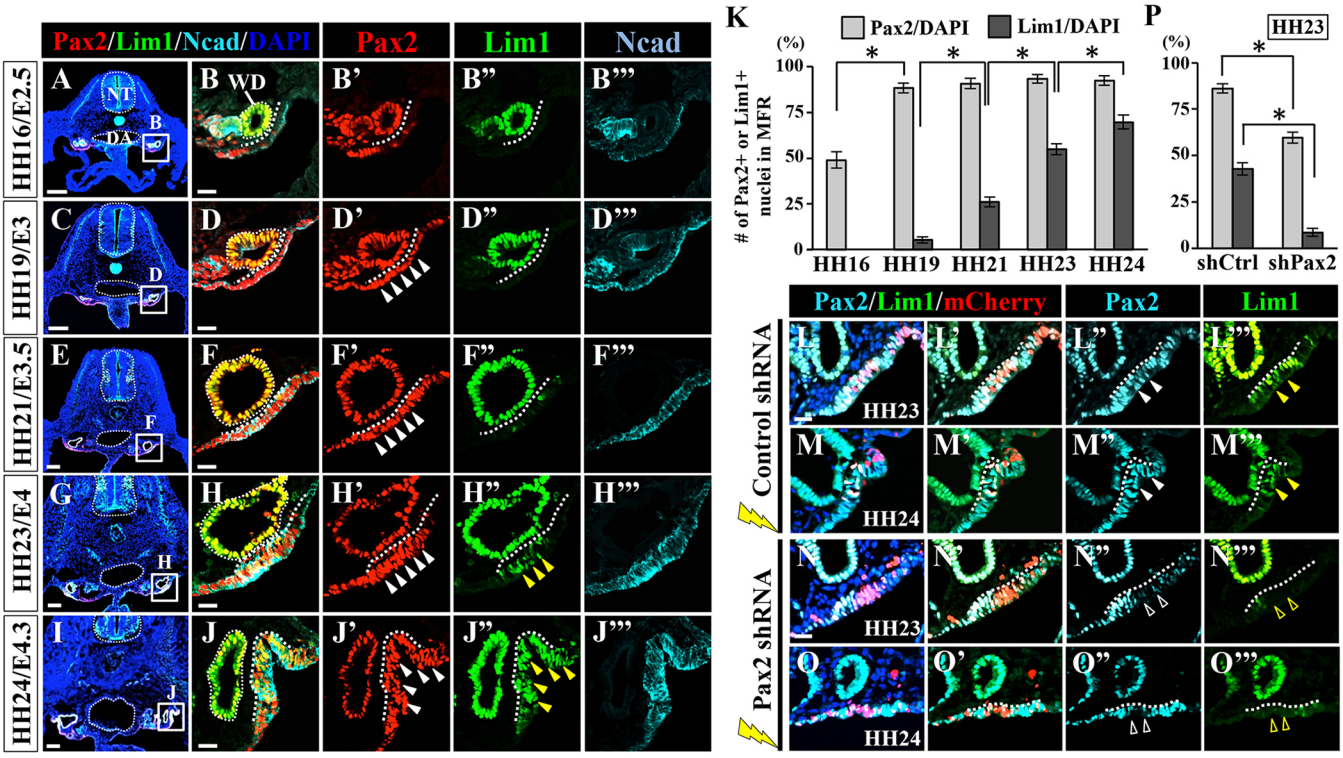

Fig. 1. Time course and requirement of Pax2 for the initiation of MD development in chicken embryos. (A-J) Transverse sections containing the MFR were stained with antibodies for Pax2 (red), Lim1 (green) and N-cadherin (Ncad; cyan). HH16/E2.5 (A-B‴), HH19/E3 (C-D‴), HH21/E3.5 (E-F‴), HH23/E4 (G-H‴) and HH24/E4.3 embryos (I-J‴) were sectioned. White and yellow arrowheads indicate Pax2 and Lim1 expression in MD precursors, respectively. Dotted lines in B,D,F,H,J denote the WD and the basal sides of the CE juxtaposing the WD. Nuclei were stained with DAPI. (K) Quantification of the number of Pax2- and Lim1-positive cells in the MFR at the five stages indicated (n=14 MFRs for each respective stage). Error bars represent s.e.m. *P<0.01. (L-O‴) Plasmids carrying control short-hairpin RNA (control shRNA; L-M‴) or shRNA against Pax2 (Pax2 shRNA; N-O‴) were co-electroporated with pCAGGS-H2B-mCherry into the MFR (n=10 each). Misexpression of Pax2 shRNA resulted in downregulation of both Pax2 and Lim1 proteins (open arrowheads in N″,N‴,O″ and O‴), and caused an invagination defect (O). (P) Quantification of the number of Pax2- and Lim1-positive cells in control shRNA-electroporated and Pax2 shRNA-electroporated MFR in HH23 embryos. Error bars represent s.e.m. *P<0.01. DA, dorsal aorta; NT, neural tube. Scale bars: 100 µm (A,C,E,G,I); 20 µm (B,D,F,H,J,M,O).

Development (2016) 143, 3549-3559 doi:10.1242/dev.137067

reduced not only Pax2 but also Lim1 expression levels in the MFR, whereas scrambled control shRNA did not yield significant effects (Fig. 1L-P). Furthermore, in the shPax2-treated embryos at HH24, invagination of the MFR was abrogated (Fig. 1M,O). These data suggest that Pax2 is a key regulator for early chicken MD development, and that Lim1 acts downstream of Pax2, as seen in mouse pronephros development.

We next investigated the regulation of Pax2 expression in MD precursors. We focused on BMP signaling because it is known to activate Pax2 expression during intermediate mesoderm (IMM) development in chickens (James and Schultheiss, 2005). We found that three members of this family, *Bmp2*, *-4* and *-7*, were expressed in the MFR and its adjacent tissues, including the WD and mesonephric tubules (Fig. S3A-I). In addition, by immunostaining with an antibody against phosphorylated Smad1/5/8 (pSmad), we found that MFR cells responded to BMP signals at HH19, but not HH16, concomitantly with the increase in number of Pax2-positive cells (Fig. S3J-L). To test whether BMP signaling would indeed be required for the Pax2 expression in early MD development, noggin, an inhibitor of BMP signaling, was introduced into the MFR by electroporation. When a control plasmid expressing ZsGreen1 was electroporated, the expression of Pax2 and Lim1 in the CE and the following MD invagination were unaffected (Fig. 2A-D″,L). By contrast, noggin electroporation caused a reduction of Pax2 and Lim1 signals and also a disruption of MD invagination (Fig. 2E-H″,L). We also noticed that BMP inhibition blocked the epithelial thickening of the MFR that would normally occur prior to invagination (Fig. 2F-F″,H-H″). pSmad staining was also markedly diminished in the noggin-treated MFR (Fig. 2I-K), confirming that this treatment did indeed block the activation of BMP signaling. To

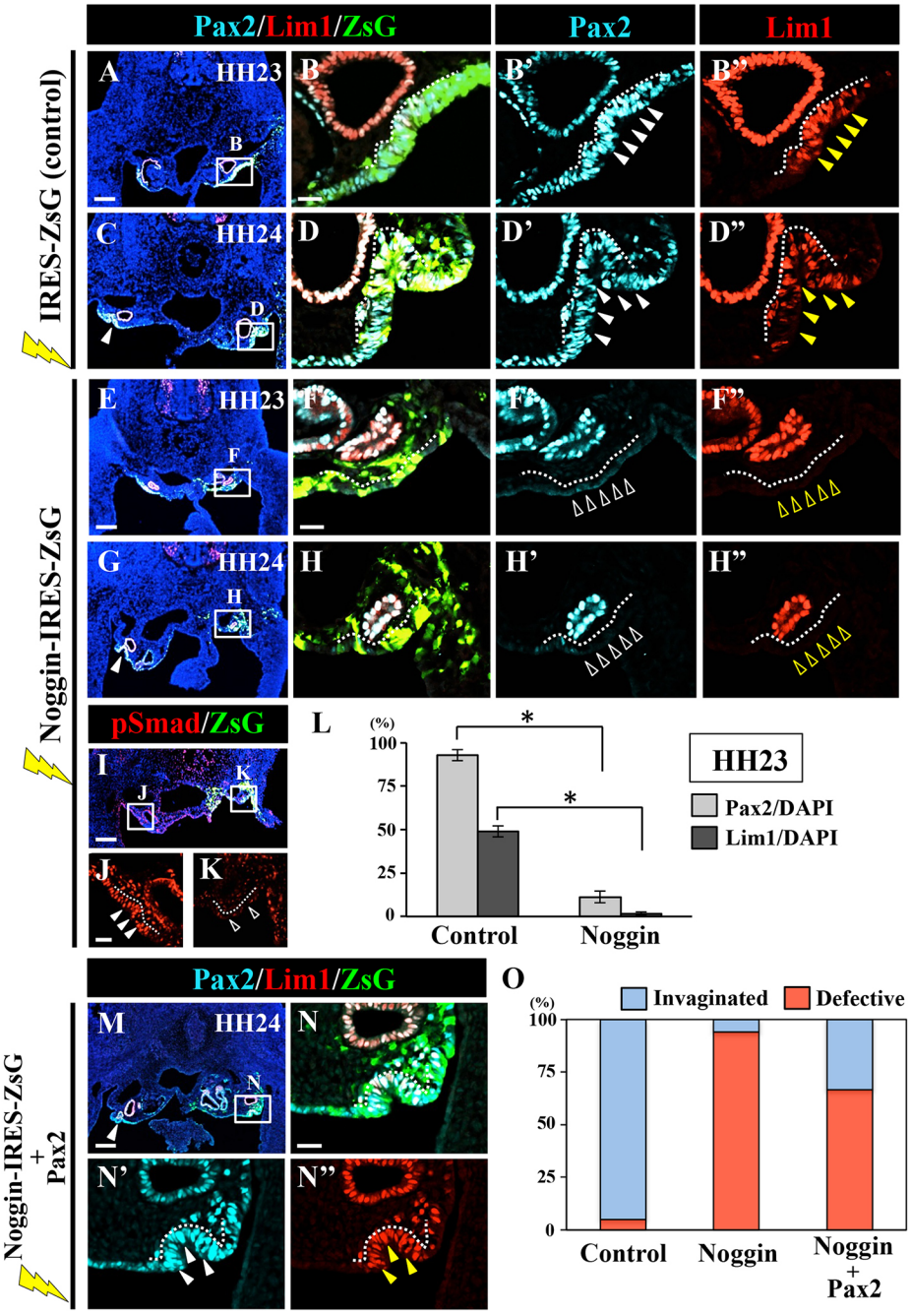

Fig. 2. BMP signaling is required for MD specification by regulating Pax2 expression in CE. (A-H″) Transverse views of embryos into which IRES-ZsG-expressing plasmids (control; A-D″; *n*=19 for each stage) or noggin-IRES-ZsG-expressing plasmids (E-H″; *n*=16 for each stage) were electroporated. White and yellow arrowheads mark Pax2 and Lim1 proteins in the MFR, respectively, at both HH23 (B′,B″) and HH24 (D′,D″). IRES-ZsG-electroporated cells initiated the invagination at HH24 as seen in a contralateral site (white arrowhead in C). White and yellow open arrowheads represent a loss of Pax2 and Lim1 expression, respectively, in noggin-electroporated embryos (F′,F″,H′,H″). Note that the MD invagination occurred correctly in the contralateral side at HH24 of noggin-electroporated embryos as marked by the white arrowhead in G. (I-K) Immunostaining of phosphorylated Smad1/5/8 (pSmad) in HH23 noggin-electroporated embryos. Open arrowheads in K show abrogated BMP signals by misexpression of noggin in the MFR. Arrowheads in J indicate pSmad signals in the contralateral side. (L) Quantification of the number of Pax2- and Lim1-positive cells in ZsG-electroporated- and noggin-electroporated MFR in HH23 embryos. Error bars represent s.e.m. **P*<0.01. (M-N″) Representative image of embryos into which Noggin-IRES-ZsG- and Pax2-expressing plasmids were co-electroporated. Introduction of Pax2 led to the restoration of Lim1 expression (yellow arrowheads in N″) and invagination of the MFR. White arrowheads in M and N′ indicate invagination of the contralateral side and Pax2 signals of the electroporated MFR, respectively. (O) Percentages of embryos displaying normal invagination (light blue) or an invagination defect (red): 95% (*n*=19/20) of IRES-ZsG-, 5.9% (*n*=1/17) of Noggin-IRES-ZsG- and 33.3% (*n*=5/15) of Noggin-IRES-ZsG- and Pax2-electroporated specimens showed normal invagination. ZsG, ZsGreen1. Dotted lines indicate basal sides of the CE juxtaposing the WD. Scale bars: 100 µm (A,E,I,M); 20 µm (B,F,J,N).

Development (2016) 143, 3549-3559 doi:10.1242/dev.137067

investigate further whether the function of BMP signaling was mediated through Pax2, *Pax2* cDNA was co-electroporated with noggin cDNA into the MFR (Fig. 2M,N-N″). In five embryos out of 15, both the Lim1 expression and its subsequent MD invagination were restored even in the absence of BMP signaling (Fig. 2M-O). Based on these data, we concluded that the BMP/Pax2 axis is crucial for early MD development.

FGF cascades are activated by BMP signaling in the MFR

To understand further the signaling pathway acting under the BMP-mediated cascade leading to Lim1 expression and the invagination of the MD, we examined other signaling pathways in the developing MD. We hypothesised that FGF signaling would be a strong candidate for the following two reasons. First, we found that FGF receptor 2 (*FGFR2*) started to be expressed in the MFR at HH23 (Fig. 3A-C) concomitantly with the onset of Lim1 expression. Second, the onset of signals for phosphorylation of ERK1/2 (pERK), a prominent marker of FGF signaling, coincided with the *FGFR2* expression in the MFR (Fig. 3D-F′). The PI3K/AKT pathway, another intracellular pathway of FGF, was not activated (Fig. S4A). As among *FGFR1*, *-2* and *-3* members, only *FGFR2* mRNA was detected in the MFR (data not shown), FGFR2 appeared to be an activator of pERK. In addition, both *FGFR2* and pERK signals were markedly downregulated by misexpression of noggin (Fig. 3G-L). Thus, in the MFR, BMP signaling triggers the FGF/ERK pathway, which, in turn, could potentially regulate Lim1 expression leading to MD invagination.

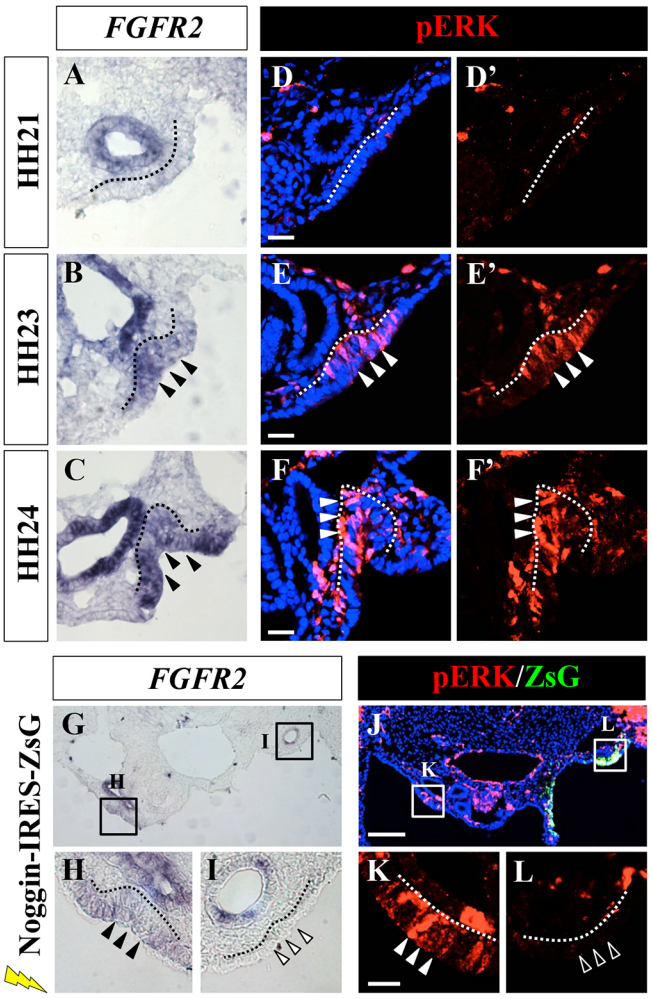

Fig. 3. Activation of FGF signaling in the MFR is regulated by BMP signaling. (A-C) *In situ* hybridization to *FGFR2* at HH21 (A), HH23 (B) and HH24 (C). *FGFR2* mRNA was observed in MFR at HH23 and HH24, as indicated by black arrowheads. (D-F′) Immunostaining against dephosphorylated ERK1/2 proteins (pERK) in HH21 (D), HH23 (E) and HH24 embryos (F). Signals for *FGFR2* and pERK were detected at HH23 and HH24 (B,C,E,F). White arrowheads indicate pERK signals in the MFR. (G-L) Transverse views of noggin-electroporated HH23 embryos. Noggin electroporation resulted in a loss of signals for *FGFR2* (I) and pERK (L) as marked by open arrowheads, compared with the signals at the contralateral sides as marked by black (H) or white (K) arrowheads. Dotted lines indicate basal sides of the CE juxtaposing the WD. Scale bars: 20 µm (D,E,F,K); 100 µm (J).

FGF signaling is required for the specification and invagination of MD precursors

To examine whether FGF signaling is indeed essential for the early MD development, a dominant-negative form of chicken FGFR2 (dnFGFR2) was introduced into the CE of HH13 embryos by *in ovo* electroporation. This manipulation abolished Lim1 expression in the MFR by HH23, and also disturbed the MD invagination seen at HH24 (Fig. 4A-D″,K). By immunostaining for cleaved caspase-3, we confirmed that these effects were not attributed to enhanced cell death (Fig. S5A-C). Notably, the inhibition of FGF signaling did not affect the Pax2 expression (Fig. 4A-D″,K), suggesting that FGF signaling acts downstream of or parallel to the BMP/Pax2 axis.

In the FGF signaling-inhibited MFR, pERK staining was markedly diminished (Fig. 4I-J′), implying that the FGF/Ras/ERK pathway is indispensable for MD development. Indeed, when Ras activity was blocked in the MFR by electroporation with dominant-negative Ras^{17N}, an unphosphorylated form of Ras (Quilliam, et al., 1994), MD invagination was disturbed and Lim1 was downregulated, but Pax2 expression remained unaffected, consistent with the dnFGFR2 experiments (Fig. 4E-H″,K). Moreover, misexpression of sprouty 2, a general inhibitor of the receptor tyrosine kinase-mediated Ras signaling (Mason et al., 2006), also disturbed both the Lim1 expression and MD invagination (Fig. S6A-E).

To investigate whether FGF/Ras/ERK signaling acted through Lim1, and whether Lim1 expression would be sufficient for inducing MD invagination, *dnFGFR2* and *Lim1* cDNAs were co-electroporated into the MFR (Fig. 4L-M″). In these embryos at HH24, invagination was restored in a manner comparable to the contralateral side (Fig. 4L-N). We conclude that FGF signaling through the Ras/ERK pathway plays a crucial role in MD specification and invagination by regulating Lim1 expression.

We confirmed that the distorted MD formation caused by a series of gene electroporations was not due to maturation delay of the tissues. For instance, in noggin- or dnFGFR-electroporated embryos, neither Lim1 expression nor MD invagination was observed even at HH25 (data not shown).

FGF signaling regulates apical constriction, breakdown of basement membrane, and epithelial thickening during MD invagination

We next explored the cellular mechanisms mediated by FGF signaling in controlling epithelial invagination. It is widely accepted that epithelial invagination is initiated by apical constriction, a process in which myosin II and F-actin form contractile networks (Martin and Goldstein, 2014), and non-muscle myosin II is activated only when the regulatory myosin light chain is phosphorylated (pMLC) (Schliwa and Woehlke, 2003). We found that pMLC was localized predominantly in the apical side of MFR

Development (2016) 143, 3549-3559 doi:10.1242/dev.137067

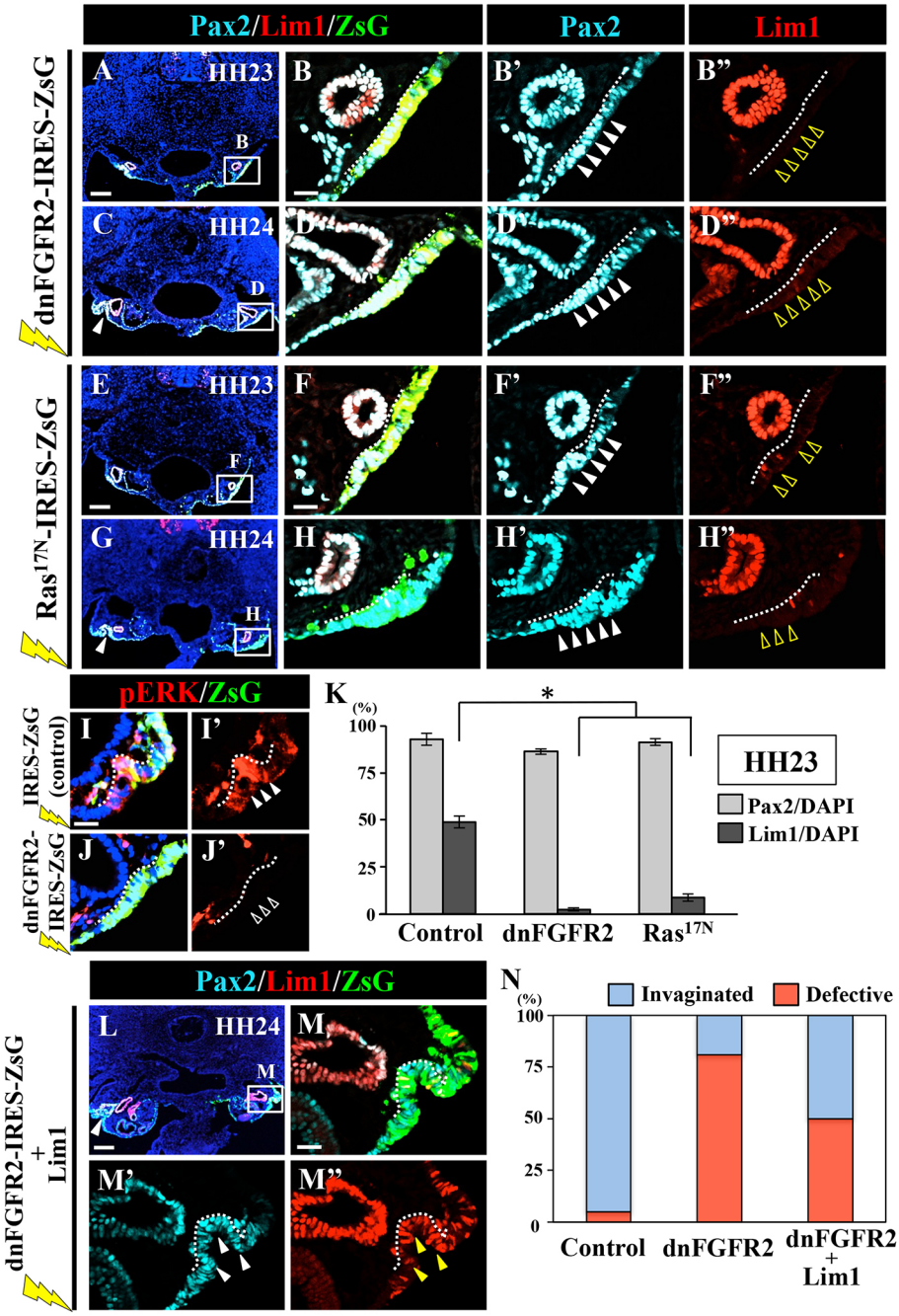

Fig. 4. FGF signaling through the Ras/ERK pathway controls early MD development by regulating expression of Lim1, but not Pax2. (A-H″) Transverse views of embryos electroporated with dnFGFR2 (A-D″; *n*=17 for each stage) or dnRas (Ras17N; E-H″; *n*=11 for each stage). Both treatments abrogated Lim1 expression (yellow open arrowheads in B″,D″,F″, H″), but did not affect Pax2 (white arrowheads in B′,D′,F′,H′) at HH23 and HH24. The invagination was disrupted in both cases (arrowheads in C,G). (I-J′) Sections of ZsG- (I,I′) or dnFGFR2- (J,J′) electroporated embryos stained with antibodies for pERK (red). Signals for pERK were not detected in dnFGFR2-treated MFR as indicated by open arrowheads in J′. (K) Quantification of the number of Pax2^{+} and Lim1^{+} cells in ZsG-, dnFGFR2- or dnRas-electroporated MFR in HH23 embryos. Error bars represent s.e.m. **P*<0.01. (L-M″) Representative images of embryos into which dnFGFR2-IRES-ZsG- and Lim1-expressing plasmids were co-electroporated. Misexpression of Lim1 rescued invagination of the MFR (arrowheads in M′ and M″). (N) Percentages of embryos displaying normal invagination (light blue) or an invagination defect (red): 95% (*n*=19/20) of IRES-ZsG-, 19% (*n*=4/21) of dnFGFR2-IRES-ZsG- and 50% (*n*=8/16) of dnFGFR2-IRES-ZsG- and Lim1-electroporated MFRs showed normal invagination. Dotted lines indicate basal sides of the CE juxtaposing the WD. Scale bars: 100 µm (A,E,L); 20 µm (B,F,I,M).

cells when MD invagination initiated (HH23), although this localization was not yet seen at HH21 (Fig. 5A-D″). We further investigated whether the apical localization of pMLC was regulated by FGF signaling. When FGF signaling was inhibited by dnFGFR2, pMLC localization in MFR cells was altered to punctate patterns, and the length of pMLC-positive signals in the MFR decreased significantly (Fig. 5E-H″,M-O). Similarly, the apical accumulation of F-actin and N-cadherin was disturbed by the depletion of FGF signaling (Fig. S7A,B; Fig. 5F,H). Thus, the apical actin-myosin constriction, which would drive MD invagination, is positively regulated by FGF signaling.

After invagination, MD cells are known to migrate collectively toward the cloaca along the WD (Dohr and Tarmann, 1984; Guioli et al., 2007; Orvis and Behringer, 2007). We found that during this migration, mesenchymal-like cells located at the caudal tip of MD extended pseudopodia actively (Fig. S8A-D; Movie 1), resembling cells undergoing epithelial-to-mesenchymal transition (EMT). Because the initial step of EMT is accompanied by breakdown of the basement membrane (BM) (Nakaya et al., 2008), we examined the distribution of the BM during MD invagination by immunostaining for laminin1, a major component of the BM. The laminin1-positive layer deposited at the basal side of the early MFR disappeared by HH23 (Fig. 5I-J′), and this BM breakdown was restricted to the region of MD invasion. Importantly, FGF signaling in the MFR was essential for this process as the inhibition of FGF signaling resulted in a retention of the laminin1-positive layer (Fig. 5K-′L,N-N″,P).

Concomitantly with the apical constriction and BM breakdown, the MFR undergoes tissue thickening, which is another hallmark of epithelial invagination (Kondo and Hayashi, 2015). We observed

Development (2016) 143, 3549-3559 doi:10.1242/dev.137067

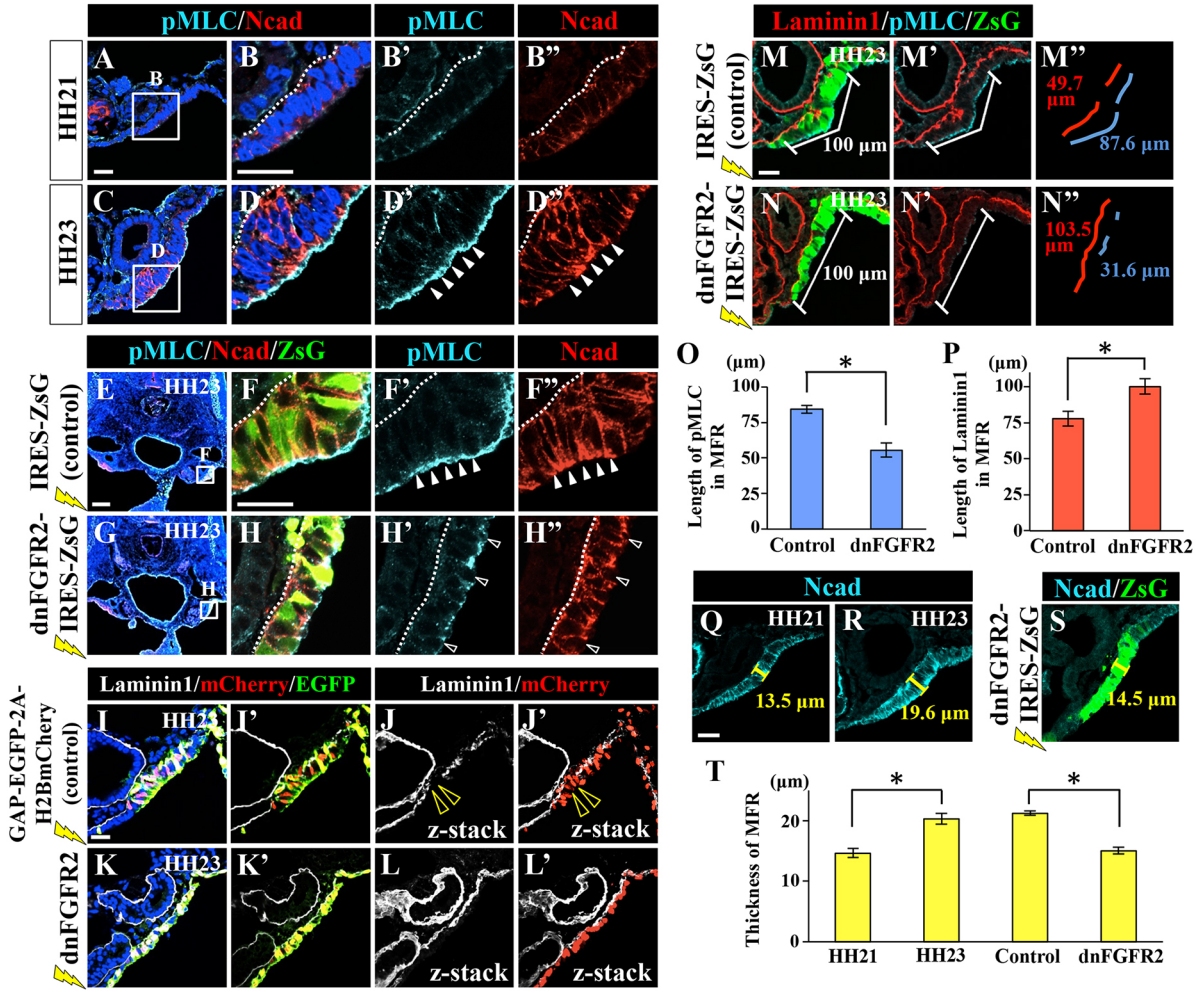

Fig. 5. FGF signaling is required for apical accumulation of pMLC, breakdown of Laminin1/BM and thickening of the MFR at the onset of MD invagination. (A-D″) Transverse sections of HH21 and HH23 embryos immunostained for pMLC (cyan) and N-cadherin (Ncad; red). White arrowheads in D′ and D″ indicate apically enriched pMLC and N-cadherin, respectively, in MD precursors at HH23. (E-H″) Sections of ZsG- (E-F″; *n*=17) or dnFGFR2- (G-H″; *n*=9) electroporated HH23 embryos. dnFGFR2-electroporated cells show a disruption of apical accumulation of pMLC and N-cadherin as indicated by open arrowheads in H′ and H″. Arrowheads in F′ and F″ indicate apically enriched pMLC and N-cadherin, respectively. (I-L′) Sections of HH23 embryos into which only GAP-EGFP-P2A-H2B-mCherry (I-J′; *n*=7), or both GAP-EGFP-P2A-H2B-mCherry and dnFGFR2 (K-L′; *n*=7) were electroporated. Immunostaining against Laminin1 (white) demonstrated that normal MD precursors broke down Laminin1/BM (yellow open arrowheads in J,J′), and that this breakdown did not take place when FGF signaling was inhibited (L,L′). Images in I,L are of confocal *z*-stack images in which 20 slices with *z*-spacings of 0.5 µm were stacked. (M-N″) Total length of pMLC- or Laminin1-positive signals in the MFR, where IRES-ZsG (M) or dnFGFR2-IRES-ZsG (N) was introduced, was measured (indicated by brackets). (O,P) pMLC (O) and Laminin1 (P) length in control (*n*=17) or dnFGFR2-electroporated MFR (*n*=9). Error bars represent s.e.m. **P*<0.05. (Q-T) Measurement of the thickness of MFRs. (Q-S) Thickness of HH21 (13.5 µm; Q), HH23 (19.6 µm; R), ZsG-electroporated HH23 and dnFGFR2-electroporated HH23 (14.5 µm; S) MFRs measured according to N-cadherin signal. (T) Graph representing thickness of HH21 (*n*=17), HH23 (*n*=19), ZsG-electroporated HH23 (control; *n*=14) and dnFGFR2-electroporated HH23 (*n*=16) MFRs. Error bars represent s.e.m. **P*<0.01. Dotted lines indicate the basal sides of the CE juxtaposing the WD. Scale bars: 100 µm (E); 20 µm (A,B,F,I,M,Q).

that the thickness (height) of the MFR increased from HH21 to HH23 (13.5 µm to 19.6 µm; Fig. 5Q,R,T). However, the height of dnFGFR2-electroporated MFR (14.5 µm; Fig. 5S) analyzed at HH23 was smaller than the control, suggesting that FGF signaling also regulates the thickening of MFR (Fig. 5S,T). Taken together, these data indicate that FGF signaling controls the onset of MD invagination by regulating a series of cellular and molecular machineries.

We further sought an intracellular modulator, which regulates MD invagination. In general, epithelial invagination is often mediated by Rho family small GTPases (Martin and Goldstein, 2014), and Rac1 has indeed been reported to be involved in salivary gland invagination in *Drosophila* (Pirraglia et al., 2006). To know whether the activity of Rac1 is important for MD invagination in chickens, a dominant-negative form of Rac1 (dnRac1) was electroporated into the MFR. This manipulation caused aberrant invagination of the MD concomitantly with the disruption of apical accumulation of pMLC and breakdown of laminin1 (Fig. S9A-F). By contrast, MFR thickening and Lim1 expression in the MFR were unaffected (Fig. S9A,B,G). Thus, Rac1 function is required for MD invagination by acting through the regulation of actomyosin, and not for earlier events such as MFR specification.

The WD is necessary for the activation of FGF signaling in the MFR

Because the MFR is juxtaposed to the WD, we hypothesized that the WD would define the MFR territory in the CE. To test this idea, we surgically ablated unilaterally a WD that had been

Development (2016) 143, 3549-3559 doi:10.1242/dev.137067

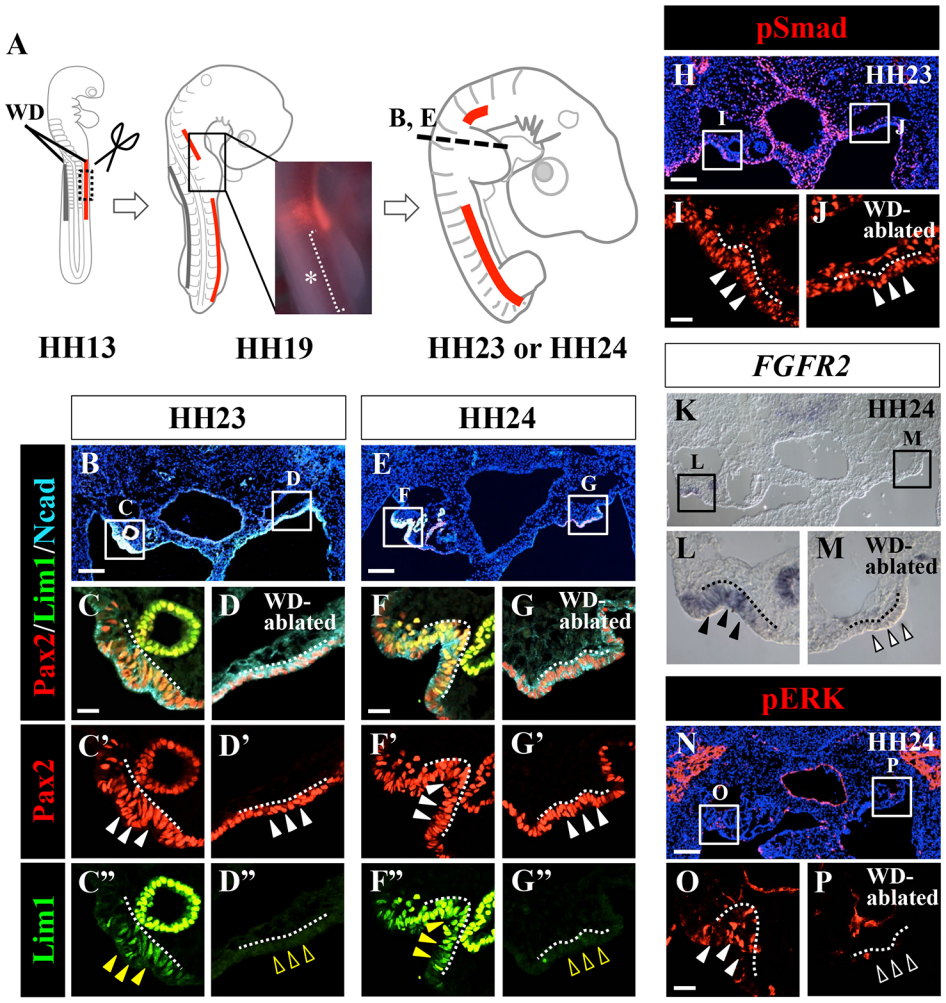

Fig. 6. WD participates in the activation of the FGF/Lim1 pathway in the MFR. (A) The PKH26-labeled WD (red) was dissected out from HH13 embryos at the presumptive forelimb level. Asterisk and white dashed bracket indicate that WD was successfully removed. WD-ablated embryos were allowed to develop until HH23 or HH24 (*n*=12 for each stage). (B-G″) Transverse sections, corresponding to the dashed line in A, were stained with antibodies for Pax2, Lim1 and N-cadherin (Ncad). In WD-ablated sides of HH23 (D-D″) and HH24 (G-G″) embryos, cells in the MFR expressed Pax2, but not Lim1, as indicated by white arrowheads and yellow open arrowheads, respectively. (H-P) Transverse views of WD-ablated embryos showing signals for pSmad (H-J), *FGFR2* mRNA (K-M) and pERK (N-P). pSmad signals in the WD-ablated side were comparable to those of the contralateral side, whereas signals for *FGFR2* and pERK were drastically diminished by WD ablation (open arrowheads in M,P). Arrowheads in I,J indicate pSmad signals in the contralateral and WD-ablated sides, respectively. Arrowheads in L, O indicate *FGFR2* mRNA and pERK signals in the contralateral sides, respectively. Dotted lines indicate basal sides of the CE juxtaposing the WD. Scale bars: 100 µm (B,E,H,N); 20 µm (C,F,I,O).

labeled with a fluorescent dye (Fig. 6A). In the MFR of the untreated side, normal expression of Pax2 and Lim1 was observed at both HH23 and HH24, and the MD rudiment started the invagination correctly at HH24 (Fig. 6B-C″,E-F″). By contrast, neither Lim1 expression nor invagination was seen in the MFR of the WD-ablated side (Fig. 6B,D-D″,E,G-G″). Notably, whereas the WD ablation did not affect Pax2 expression or pSmad (Fig. 6D-D″,G-G″,H-J), it abrogated *FGFR2* mRNA expression and pERK staining in the MFR (Fig. 6K-P). We therefore conclude that MD-WD interactions play an indispensable role in the FGF signaling that determines and specifies the MFR.

DISCUSSION

We have determined the molecular and cellular mechanisms by which early MD morphogenesis is regulated. BMP, FGF and WD-derived signals act in a spatiotemporally regulated manner both for the sequential activation of the Pax2 and Lim1 genes and for changes in cell behavior to initiate MD invagination. As outlined in Fig. 7, early MD morphogenetic processes can be divided into three major steps. Step 1 is the pre-specification stage of MD precursors during which BMP-mediated Pax2 expression commences in the CE. These events do not require a WD-derived signal. Step 2 includes Lim1 expression regulated by FGF and WD-derived signaling, and this process leads to the specification of MD precursors. At Step 3, the specified MD invaginates under the direction of apical constriction of the MFR epithelium. Thus, during early MD morphogenesis, paracrine signals including inter-epithelial communications regulate activities of transcription factors in a temporospatially controlled manner, leading to a dynamic change in cell behavior. The delineation of these mechanisms has been enabled by the high amenability of chicken embryos, whereby gene activity in the presumptive MD can specifically be manipulated. Studies on MD development were previously conducted mainly in transgenic mice. Although these studies showed the requirements for the *Pax2* and *Lim1* genes in MD morphogenesis at relatively late stages when invagination and its subsequent extension take place (Huang et al., 2014; Torres et al., 1995), the lack of MD precursor-specific conditional transgenic lines has hampered analyses of the earlier specification stages of MD development.

Step 1: The BMP-Pax2 pathway plays a crucial role in the pre-specification of MD precursors

The BMP-mediated elevation of Pax2 expression marks pre-specified MD precursors. The Pax2-positive area in the CE spans a region broader than the MFR. At the stage when Pax2 expression starts, the expression level of BMPs in the presumptive MFR is faint whereas BMP2 is abundantly expressed in the WD. However, as WD-specific ablation did not affect Pax2 or pSmad levels in the CE, it is probable that the presumptive MFR does not require high activity of BMPs, and that the moderate level of BMPs produced by the CE itself is sufficient for the self-activation of Pax2.

Development (2016) 143, 3549-3559 doi:10.1242/dev.137067

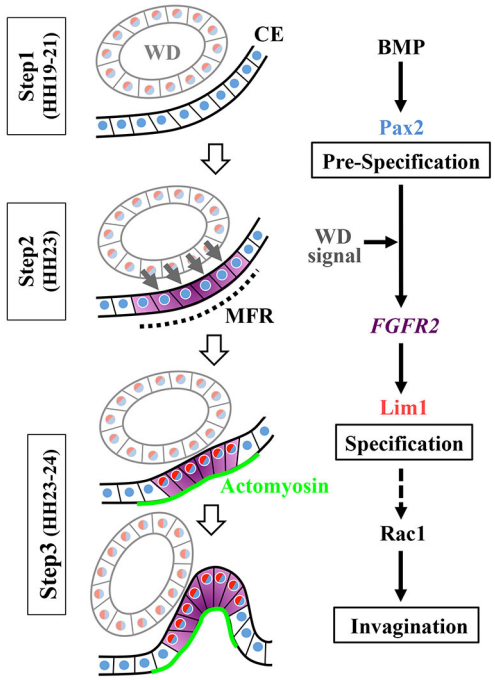

Fig. 7. Schematic model showing the cellular and molecular mechanisms underlying early MD development. The early MD morphogenetic processes consist of three major steps. Step 1 (HH19-21): BMP signaling activates the expression of Pax2 in the CE cells (blue). These Pax2-positive cells are pre-specified MD precursors. Step 2 (HH23): both the BMP/Pax2 pathway and WD-derived signals (gray arrows) are required for the induction of *FGFR2* expression (purple). The activated FGF signaling, in turn, triggers Lim1 expression in MD precursors (red). Step 3 (HH23-24): specified MD precursors (Pax2/Lim1 double-positive cells) undergo invagination that is directed by apical constriction of MFR epithelium. The apical constriction is regulated by FGF-originated cascades, and involves Rac1 and rearrangement of the actomyosin cytoskeleton.

A requirement of moderate levels of BMP for Pax2 expression has also been shown previously in the context of specification of the intermediate mesoderm (James and Schultheiss, 2005; Tonegawa et al., 1997).

A crucial role for Pax2 in the MD formation was previously reported in knockout mice (Bouchard et al., 2002; Torres et al., 1995). However, as Pax2 is expressed in both MD and WD, which were thought to interact each other, it remained unknown whether Pax2 acts cell-autonomously or non-cell-autonomously in this context. In our current study, we knocked down Pax2 specifically in the CE leaving the WD intact, and found that this manipulation entirely abrogated the subsequent morphogenesis of the MD. Furthermore, because the expression of endogenous Lim1 is upregulated in the MFR by simultaneous transfection with *Pax2* and noggin, we can conclude that Pax2 activates Lim1 expression independently of BMP signaling. Thus, the cell-autonomous function of Pax2 in the CE, but not in the WD, is required for the early specification of the MD.

Step 2: The FGF/Lim1 axis in the specification of MD precursors

Previously, genetic experiments in the mouse demonstrated that Lim1 is required for maintenance and growth of MD cells in a cell-autonomous manner (Huang et al., 2014; Kobayashi et al., 2005, 2004). In the current study, we have examined the upstream signals that regulate Lim1 during MD specification, and found that Lim1 expression is triggered by FGF activity, which, in turn, is regulated by the BMP/Pax2 axis. In addition to the requirement of Lim1 for MD specification, we have demonstrated that Lim1 is sufficient for MD invagination by acting cell-autonomously. When Lim1 is misexpressed in the MFR, MD invagination is induced even though FGF signaling is depleted (Fig. 4L-N).

We have shown that FGF signaling in MFR cells is transmitted through FGFR2. The most likely ligands involved in this step are FGF2, FGF8 and/or FGF9, all of which are expressed in the mesonephric region, and are known to have high affinity for FGFR2 (Antin et al., 2014; Martin et al., 2006; Yoshioka et al., 2005). Our study has also revealed that FGF signaling in the MFR is intracellularly transduced through the Ras/ERK pathway but not the PI3K/AKT pathway (Fig. 4; Fig. S4). Interestingly, once MD starts its extension, the PI3K pathway becomes prominent, and this activation is known to be required for MD extension (Fujino et al., 2009). How the switch from Ras/ERK to PI3K/AKT signaling is regulated remains unknown.

Positive regulation of Lim1 expression by Pax2 was previously shown in the nephric lineage specification in the IMM (Bouchard et al., 2002). However, unlike the MFR, Lim1 expression does not require FGFs in the IMM (Atsuta and Takahashi, 2015). Elucidation of how the FGF signal in the MFR is integrated into the Pax2-mediated regulation of the *Lim1* gene requires further investigation.

Another important finding obtained in this study is that the activity of the FGF/Lim1 axis in the MFR requires a WD-derived signal in addition to Pax2 activity, as WD ablation abolished expression of *FGFR2*, pERK and Lim1 in the MFR (Fig. 6). The molecular nature of the WD-derived signal is yet to be identified, although BMPs are unlikely because pSmad signaling is not diminished by WD removal (Fig. 6H-J). Similarly, Wnt9b, also expressed in the WD, is not a strong candidate for the WD factor as it is known that MD specification remains unaffected in *Wnt9b* knockout mice (Carroll et al., 2005). Wnt4 expressed in the mesonephric portion is also not promising because the initiation step of murine MD occurs independently of Wnt4 (Prunskaite-Hyyrylainen et al., 2016).

Step 3: Cytoskeletal rearrangement during invagination of the MD

The molecular cascade originating from the BMP/Pax2 and FGF/Lim1 axes culminates in a drastic change in epithelial morphogenesis, initiating the process of invagination (Fig. 7).

Invagination of the MFR is accompanied by the apical constriction of acto-myosin structures, breakdown of basement membrane (laminin1), and epithelium thickening. FGF-mediated actions during epithelial invagination were previously described for cytoskeletal rearrangements in the otic placode in chickens (Sai and Ladher, 2008), and also for mechanosensory organ formation in fish (Harding and Nechiporuk, 2012). Thus, the FGF/Ras/ERK pathway might be a part of a general mechanism that governs epithelial invagination. We have demonstrated in the current study that the FGF/Ras/ERK pathway triggers the phosphorylation of MLC, an executer of the apical constriction. This regulation might be through Rac1 activity, although Rac1 appears not to regulate the MFR thickening. RhoA might be another important modulator of the MFR invagination as it is known that *RhoA* mRNA expression and the apical positioning of Rho-associated kinase are regulated by the FGF/Ras/ERK pathway in other developmental contexts (Chauhan et al., 2011; Harding and Nechiporuk, 2012; Hardy et al., 2011; Nakaya et al., 2008). Indeed, we have observed that the RhoA protein is predominantly localized in the apical region of the MFR in HH23 embryos (data not shown).

Development (2016) 143, 3549-3559 doi:10.1242/dev.137067

Participation of WD-derived signals in MD specification

Because the WD is localized in close proximity to the MFR, WD-MFR interactions were expected to play important roles in the MD formation. Indeed, it was previously shown that the WD is essential for MD extension after its invagination in chickens and mice (Carroll et al., 2005; Gruenwald, 1941; Orvis and Behringer, 2007). In the current study, we have demonstrated that although the WD-derived signal is dispensable for the BMP-mediated Pax2 expression in pre-specified MD, this signal is required for the subsequent activation of the FGF/Lim1 axis. Thus, inter-epithelial communications between the early MD and the WD act in a temporally regulated manner.

Interplay between the WD and the CE has also been reported in the nephric region at more posterior levels (18th-22nd somites) (Yoshino et al., 2014). In this report, the authors showed that in the absence of the WD, the overlying CE fails to undergo proper epithelialization, and also that these WD-CE interactions are mediated by fibronectin produced by the WD. Whether fibronectin serves as a WD-derived signal for the MFR specification found in the current study awaits further investigation.

Conserved mechanisms of MD formation during animal evolution

It is noteworthy that *LIM1* missense mutations and *FGFR2* mutations are seen in humans with Müllerian aplasia and endometrial carcinoma, respectively (Gatius et al., 2011; Kobayashi and Behringer, 2003). The role of Lim1 in the formation of female reproductive organs appears to be conserved not only among vertebrates, but also during animal evolution, as *lin-11* and *egl-38*, the orthologs of *Lim1* and *Pax2/5/8*, respectively, are required for uterine development in *Caenorhabditis elegans* (Chamberlln et al., 1997; Kobayashi and Behringer, 2003; Newman et al., 1999).

The molecular mechanisms unveiled in this study will open the way for further investigations into how the formation of female reproductive tract emerged during animal evolution, and may also ultimately help in the development of therapeutic treatments for diseases related to the female reproductive organs, including Müllerian aplasia.

MATERIALS AND METHODS

Experimental animals

Fertilized chicken (*Hypeco nera*) eggs were obtained from Shiroyama-Keien (Sagamihara, Japan). Embryos were staged according to Hamburger and Hamilton (1992). All the animal experiments were performed under the ethical guidelines of Kyoto University.

Immunohistochemistry

For immunological staining on histological sections, the following antibodies were used as described by Atsuta and Takahashi (2015): mouse anti-laminin1 [Developmental Studies Hybridoma Bank (DSHB), 3H11], mouse anti-Lim1 (DSHB, 4F2) and rabbit anti-pERK1/2 (Cell Signaling, #4370). Anti-pSmad1/5 rabbit polyclonal antibody (Cell Signaling, #9516) was used as reported by Saito et al. (2012). The following antibodies were also used: rabbit anti-Pax2 (1/500; Covance, PRB-276P), rat anti-N-cadherin (1/300; TAKARA, NCD-2), rabbit anti-phospho AKT (1/100; Ser473, Cell Signaling, #4058), rabbit anti-cleaved caspase-3 (1/300; Promega, #9661), rabbit anti-phospho-myosin light chain (1/200; Ser19, Cell Signaling, #3671), mouse anti-RhoA (1/100; 26C4, Santa Cruz, sc-418). Alexa Fluor 647 phalloidin (Cell Signaling) was added to the solution containing a secondary antibody to stain filamentous actin. Sections treated with antibodies were also exposed to DAPI (Sigma). Fluorescent images were acquired using an A1R confocal laser scanning microscope (Nikon) and processed with NIS-Elements software (Nikon).

Expression vectors

pCAGGS-H2B-mCherry, pCAGGS-GAP43-EGFP and pCAGGS-GAP43-tdTomato were described by Atsuta et al. (2013). pSilencer-Pax2 shRNA and pSilencer-scrambled shRNA were as reported by Watanabe et al. (2007). pCAGGS-GAP43-EGFP-P2A-H2BmCherry was described by Atsuta and Takahashi (2015). For pT2A-CAGGS-IRES2-ZsGreen1 (pT2A-CAG-IRES-ZsG), the blunted IRES2-ZsGreen1 fragment derived from pIRES2-ZsGreen1 plasmid (Clontech) was subcloned into an *Eco*RV site of pT2A-CAGGS vector (Murai et al., 2015; Urasaki et al., 2006). To obtain pT2A-CAGGS-Noggin-IRES-ZsG, the open reading frame (ORF) region of noggin was subcloned into *Mlu-Nhe* sites, upstream of the IRES coding sequences of pT2A-CAGGS-IRES-ZsG, allowing for the bicistronic expression of ZsG and noggin. For pT2A-CAGGS-dnFGFR2-IRES-ZsG and pCAGGS-dnFGFR2, a kinase-deleted form of chicken FGFR2c (Havens et al., 2008) was isolated, and subcloned into *Mlu-Nhe* sites of pT2A-CAGGS-IRES-ZsG or pCAGGS. cDNA of sprouty2, gifted from Dr D. Saito (Tohoku University), was subcloned into *Mlu-Nhe* sites of pT2A-CAGGS-IRES-ZsG to obtain pT2A-CAGGS-Sprouty2-IRES-ZsG. For pT2A-CAGGS-Ras^{17N}-IRES-ZsG, Ras^{17N} ORF provided by Dr T. Yoshino (Kyushu University) was subcloned into an *Eco*RI site of pT2A-CAGGS-IRES-ZsG. For pT2A-CAGGS-dnRac1-IRES-ZsG, dnRac1, gifted from Dr K. Kaibuchi (Nagoya University), was subcloned into *Mlu-Nhe* sites of pT2A-CAGGS-IRES-ZsG. Both pCAGGS-Pax2 and pCAGGS-Lim1 were gifted from Dr H. Nakamura (Tohoku University).

In ovo electroporation

The method of *in ovo* DNA electroporation into the CE was performed as previously reported (Guioli et al., 2007), with slight modifications. Briefly, DNA plasmids were prepared at 2 µg/µl, and injected into the coelomic cavity of HH13 embryos. An electric pulse of 50 V, 50 µs, was given, followed by six pulses of 11 V, 25 ms, with 250-ms interval between pulses (CUY21EX, BEX). *In ovo* electroporation into WD cells was performed as previously described (Atsuta et al., 2013).

Probes and *in situ* hybridization

Chicken cDNA fragments for BMP2, BMP4 and BMP7 were gifted from Dr D. Saito (Tohoku University). cDNA of FGFR2 was described by Atsuta and Takahashi (2015). Digoxigenin-labeled probes were prepared according to the manufacturer's instruction (Roche). Section *in situ* hybridizations were performed as previously described (Yoshino et al., 2014).

Ablation of WD

WD was visualized by PKH26-labeling (Sigma) at HH10 as reported by Atsuta et al. (2013). After a 12 h incubation, the labeled WD was removed carefully using a sharpened tungsten needle under a fluorescence microscope.

Explant culture of mesonephros and time-lapse imaging

Urogenital ridges of electroporated HH26 [embryonic day (E)5] embryos were dissected in PBS, and embedded with 1% low melting point agarose (Invitrogen) in a 35-mm glass-bottom dish (Greiner). These explants were cultured with 10% FBS/DMEM (Nissui) in an incubation chamber connected to an A1R confocal laser scanning microscope for 4 h at 38°C. Time-lapse images were obtained and processed with NIS-Elements software.

Statistical analysis

P-values were obtained using a two-tailed, unpaired Student's *t*-test.

Acknowledgements

We thank Dr C. Tabin (Harvard Medical School) for careful reading of the manuscript, and Dr D. Saito (Tohoku University) for sharing plasmids and helpful discussion. We also acknowledge T. Kawachi (Kyoto University) for his technical support.

Competing interests
The authors declare no competing or financial interests.

Author contributions
Conceptualization: Y.A.; Methodology: Y.A.; Formal analysis and investigation: Y.A.; Writing - original draft preparation: Y.A.; Writing - review and editing: Y.A. and Y.T.; Funding acquisition: Y.A. and Y.T.

Funding
This work was supported by a Grant-in-Aid for Scientific Research on Innovative Areas, and a Grant-in-Aid for Challenging Exploratory Research from the Ministry of Education, Culture, Sports, Science and Technology of Japan (MEXT); the Mitsubishi Foundation; the Senshin Medical Research Foundation; and the Takeda Science Foundation. Y.A. is the recipient of a fellowship from the Naito Foundation.

Supplementary information
Supplementary information available online at
http://dev.biologists.org/lookup/doi/10.1242/dev.137067.supplemental

References

Antin, P. B., Yatskievych, T. A., Davey, S. and Darnell, D. K. (2014). GEISHA: an evolving gene expression resource for the chicken embryo. *Nucleic Acids Res.* **42**, D933-D937.
Atsuta, Y., Tadokoro, R., Saito, D. and Takahashi, Y. (2013). Transgenesis of the Wolffian duct visualizes dynamic behavior of cells undergoing tubulogenesis in vivo. *Dev. Growth Differ.* **55**, 579-590.
Atsuta, Y. and Takahashi, Y. (2015). FGF8 coordinates tissue elongation and cell epithelialization during early kidney tubulogenesis. *Development* **142**, 2329-2337.
Ayers, K. L., Cutting, A. D., Roeszler, K. N., Sinclair, A. H. and Smith, C. A. (2015). DMRT1 is required for Müllerian duct formation in the chicken embryo. *Dev. Biol.* **400**, 224-236.
Behringer, R. R., Finegold, M. J. and Cate, R. L. (1994). Müllerian-inhibiting substance function during mammalian sexual development. *Cell* **79**, 415-425.
Boualia, S. K., Gaitan, Y., Tremblay, M., Sharma, R., Cardin, J., Kania, A. and Bouchard, M. (2013). A core transcriptional network composed of Pax2/8, Gata3 and Lim1 regulates key players of pro/mesonephros morphogenesis. *Dev. Biol.* **382**, 555-566.
Bouchard, M., Souabni, A., Mandler, M., Neubüser, A. and Busslinger, M. (2002). Nephric lineage specification by Pax2 and Pax8. *Genes Dev.* **16**, 2958-2970.
Carroll, T. J., Park, J.-S., Hayashi, S., Majumdar, A. and McMahon, A. P. (2005). Wnt9b plays a central role in the regulation of mesenchymal to epithelial transitions underlying organogenesis of the mammalian urogenital system. *Dev. Cell* **9**, 283-292.
Chamberlln, H. M., Palmer, R. E., Newman, A. P., Sternberg, P. W., Balllle, D. L. and Thomas, J. H. (1997). The PAX gene egl-38 mediates developmental patterning in Caenorhabditis elegans. *Development* **124**, 3919-3928.
Chauhan, B. K., Lou, M., Zheng, Y. and Lang, R. A. (2011). Balanced Rac1 and RhoA activities regulate cell shape and drive invagination morphogenesis in epithelia. *Proc. Natl. Acad. Sci. USA* **108**, 18289-18294.
Cunha, G. R. (1975). The dual origin of vaginal epithelium. *Am. J. Anat.* **143**, 387-392.
Dohr, G. and Tarmann, T. (1984). Contacts between Wolffian and Müllerian cells at the tip of the outgrowing Müllerian duct in rat embryos. *Acta. Anat.* **120**, 123-128.
Freter, S., Muta, Y., O'Neill, P., Vassilev, V. S., Kuraku, S. and Ladher, R. K. (2012). Pax2 modulates proliferation during specification of the otic and epibranchial placodes. *Dev. Dyn.* **241**, 1716-1728.
Fujino, A., Arango, N. A., Zhan, Y., Manganaro, T. F., Li, X., MacLaughlin, D. T. and Donahoe, P. K. (2009). Cell migration and activated PI3K/AKT-directed elongation in the developing rat Müllerian duct. *Dev. Biol.* **325**, 351-362.
Gatius, S., Velasco, A., Azueta, A., Santacana, M., Pallares, J., Valls, J., Dolcet, X., Prat, J. and Matias-Guiu, X. (2011). FGFR2 alterations in endometrial carcinoma. *Mod. Pathol.* **24**, 1500-1510.
Gruenwald, P. (1941). The relation of the growing Müllerian duct to the Wolffian duct and its importance for the genesis of malformations. *Anat. Rec.* **81**, 1-19.
Guioli, S., Sekido, R. and Lovell-Badge, R. (2007). The origin of the Müllerian duct in chick and mouse. *Dev. Biol.* **302**, 389-398.
Hamburger, V. and Hamilton, H. L. (1992). A series of normal stages in the development of the chick embryo. 1951. *Dev. Dyn.* **195**, 231-272.
Harding, M. J. and Nechiporuk, A. V. (2012). Fgfr-Ras-MAPK signaling is required for apical constriction via apical positioning of Rho-associated kinase during mechanosensory organ formation. *Development* **139**, 3130-3135.
Hardy, K. M., Yatskievych, T. A., Konieczka, J. H., Bobbs, A. S. and Antin, P. B. (2011). FGF signalling through RAS/MAPK and PI3K pathways regulates cell movement and gene expression in the chicken primitive streak without affecting E-cadherin expression. *BMC Dev. Biol.* **11**, 20.
Havens, B. A., Velonis, D., Kronenberg, M. S., Lichtler, A. C., Oliver, B. and Mina, M. (2008). Roles of FGFR3 during morphogenesis of Meckel's cartilage and mandibular bones. *Dev. Biol.* **316**, 336-349.
Huang, C.-C., Orvis, G. D., Kwan, K. M. and Behringer, R. R. (2014). Lhx1 is required in Müllerian duct epithelium for uterine development. *Dev. Biol.* **389**, 124-136.
Jacob, M., Konrad, K. and Jacob, H. J. (1999). Early development of the Müllerian duct in avian embryos with reference to the human. *Cells Tissues Organs* **164**, 63-81.
James, R. G. and Schultheiss, T. M. (2005). Bmp signaling promotes intermediate mesoderm gene expression in a dose-dependent, cell-autonomous and translation-dependent manner. *Dev. Biol.* **288**, 113-125.
Kobayashi, A. and Behringer, R. R. (2003). Developmental genetics of the female reproductive tract in mammals. *Nat. Rev. Genet.* **4**, 969-980.
Kobayashi, A., Kwan, K.-M., Carroll, T. J., McMahon, A. P., Mendelsohn, C. L. and Behringer, R. R. (2005). Distinct and sequential tissue-specific activities of the LIM-class homeobox gene Lim1 for tubular morphogenesis during kidney development. *Development* **132**, 2809-2823.
Kobayashi, A., Shawlot, W., Kania, A. and Behringer, R. R. (2004). Requirement of Lim1 for female reproductive tract development. *Development* **131**, 539-549.
Kondo, T. and Hayashi, S. (2015). Mechanisms of cell height changes that mediate epithelial invagination. *Dev. Growth Differ.* **57**, 313-323.
Layman, L. C. (2013). The genetic basis of female reproductive disorders: etiology and clinical testing. *Mol. Cell. Endocrinol.* **370**, 138-148.
Martin, A. C. and Goldstein, B. (2014). Apical constriction: themes and variations on a cellular mechanism driving morphogenesis. *Development* **141**, 1987-1998.
Martín, C., Bueno, D., Alonso, M. I., Moro, J. A., Callejo, S., Parada, C., Martín, P., Carnicero, E. and Gato, A. (2006). FGF2 plays a key role in embryonic cerebrospinal fluid trophic properties over chick embryo neuroepithelial stem cells. *Dev. Biol.* **297**, 402-416.
Mason, J. M., Morrison, D. J., Basson, M. A. and Licht, J. D. (2006). Sprouty proteins: multifaceted negative-feedback regulators of receptor tyrosine kinase signaling. *Trends Cell Biol.* **16**, 45-54.
Momose, T., Tonegawa, A., Takeuchi, J., Ogawa, H., Umesono, K. and Yasuda, K. (1999). Efficient targeting of gene expression in chick embryos by microelectroporation. *Dev. Growth Differ* **41**, 335-344.
Mullen, R. D. and Behringer, R. R. (2014). Molecular genetics of Müllerian duct formation, regression and differentiation. *Sex. Dev.* **8**, 281-296.
Murai, H., Tadokoro, R., Sakai, K.-I. and Takahashi, Y. (2015). In ovo gene manipulation of melanocytes and their adjacent keratinocytes during skin pigmentation of chicken embryos. *Dev. Growth Differ.* **57**, 232-241.
Nakaya, Y., Sukowati, E. W., Wu, Y. and Sheng, G. (2008). RhoA and microtubule dynamics control cell-basement membrane interaction in EMT during gastrulation. *Nat. Cell Biol.* **10**, 765-775.
Newman, A. P., Acton, G. Z., Hartwleg, E., Horvitz, H. R. and Sternberg, P. W. (1999). The lin-11 LIM domain transcription factor is necessary for morphogenesis of C. elegans uterine cells. *Development* **126**, 5319-5326.
Orvis, G. D. and Behringer, R. R. (2007). Cellular mechanisms of Müllerian duct formation in the mouse. *Dev. Biol.* **306**, 493-504.
Pirraglia, C., Jattani, R. and Myat, M. M. (2006). Rac function in epithelial tube morphogenesis. *Dev. Biol.* **290**, 435-446.
Prunskaite-Hyyryläinen, R., Skovorodkin, I., Xu, Q., Miinalainen, I., Shan, J. and Vainio, S. J. (2016). Wnt4 coordinates directional cell migration and extension of the Müllerian duct essential for ontogenesis of the female reproductive tract. *Hum. Mol. Genet.* **25**, 1059-1073.
Quilliam, L. A., Kato, K., Rabun, K. M., Hisaka, M. M., Huff, S. Y., Campbell-Burk, S. and Der, C. J. (1994). Identification of residues critical for Ras (17N) growth-inhibitory phenotype and for Ras interaction with guanine nucleotide exchange factors. *Mol. Cell Biol.* **14**, 1113-1121.
Sai, X. and Ladher, R. K. (2008). FGF signaling regulates cytoskeletal remodeling during epithelial morphogenesis. *Curr. Biol.* **18**, 976-981.
Saito, D., Takase, Y., Murai, H. and Takahashi, Y. (2012). The dorsal aorta initiates a molecular cascade that instructs sympatho-adrenal specification. *Science* **336**, 1578-1581.
Sandbacka, M., Laivuori, H., Freitas, E., Halttunen, M., Jokimaa, V., Morin-Papunen, L., Rosenberg, C. and Aittomäki, K. (2013). TBX6, LHX1 and copy number variations in the complex genetics of Müllerian aplasia. *Orphanet J. Rare Dis.* **8**, 125.
Schliwa, M. and Woehlke, G. (2003). Molecular motors. *Nature* **422**, 759-765.
Tonegawa, A., Funayama, N., Ueno, N. and Takahashi, Y. (1997). Mesodermal subdivision along the mediolateral axis in chicken controlled by different concentrations of BMP-4. *Development* **124**, 1975-1984.
Torres, M., Gomez-Pardo, E., Dressler, G. R. and Gruss, P. (1995). Pax-2 controls multiple steps of urogenital development. *Development* **121**, 4057-4065.
Urasaki, A., Morvan, G. and Kawakami, K. (2006). Functional dissection of the Tol2 transposable element identified the minimal cis-sequence and a highly repetitive sequence in the subterminal region essential for transposition. *Genetics* **174**, 639-649.
Vainio, S., Heikkia, M., Kispert, A., Chin, N. and McMahon, A. P. (1999). Female development in mammals is regulated by Wnt-4 signalling. *Nature* **397**, 405-409.

Development (2016) 143, 3549-3559 doi:10.1242/dev.137067

Watanabe, T., Saito, D., Tanabe, K., Suetsugu, R., Nakaya, Y., Nakagawa, S. and Takahashi, Y. (2007). Tet-on inducible system combined with in ovo electroporation dissects multiple roles of genes in somitogenesis of chicken embryos. *Dev. Biol.* **305**, 625-636.

Yoshino, T., Saito, D., Atsuta, Y., Uchiyama, C., Ueda, S., Sekiguchi, K. and Takahashi, Y. (2014). Interepithelial signaling with nephric duct is required for the formation of overlying coelomic epithelial cell sheet. *Proc. Natl. Acad. Sci. USA* **111**, 6660-6665.

Yoshioka, H., Ishimaru, Y., Sugiyama, N., Tsunekawa, N., Noce, T., Kasahara, M. and Morohashi, K.-I. (2005). Mesonephric FGF signaling is associated with the development of sexually indifferent gonadal primordium in chick embryos. *Dev. Biol.* **280**, 150-161.

Supplementary materials

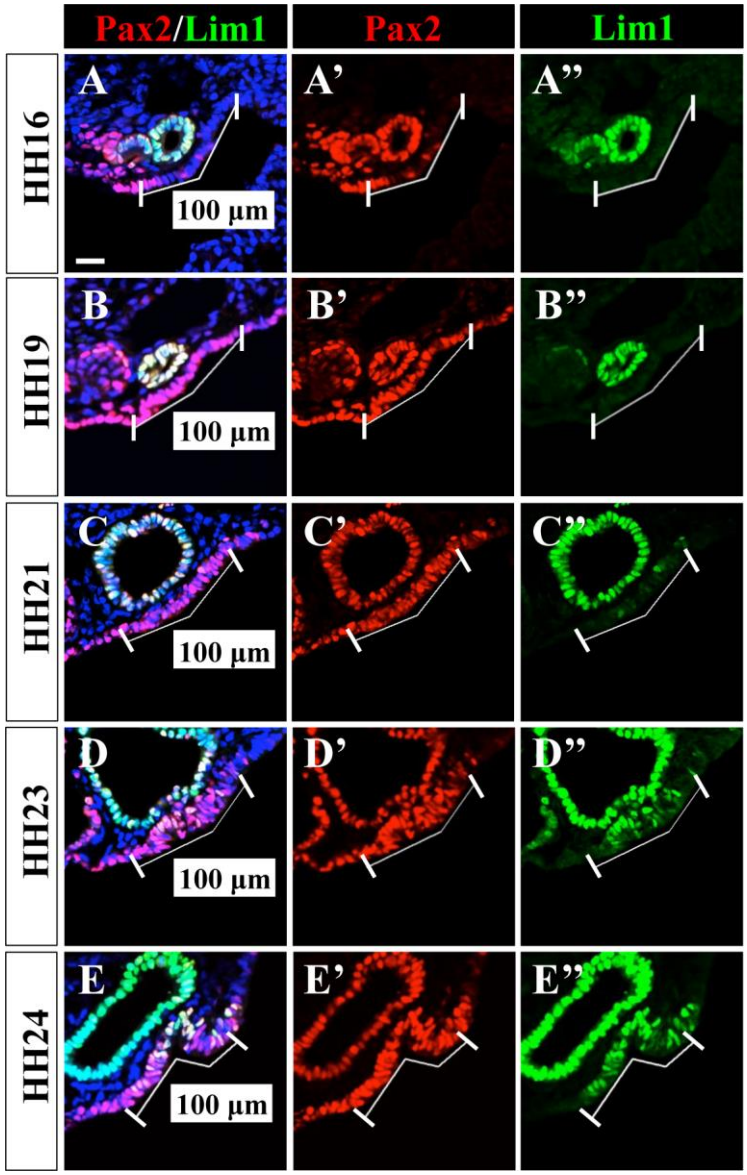

Figure S1

Definition of the Müllerian duct forming region (MFR). (A-E) The range measuring 100 µm laterally from medial edge of WD in coelomic epithelium was defined as MFR at each stage. Scale bar: 20 µm in A.

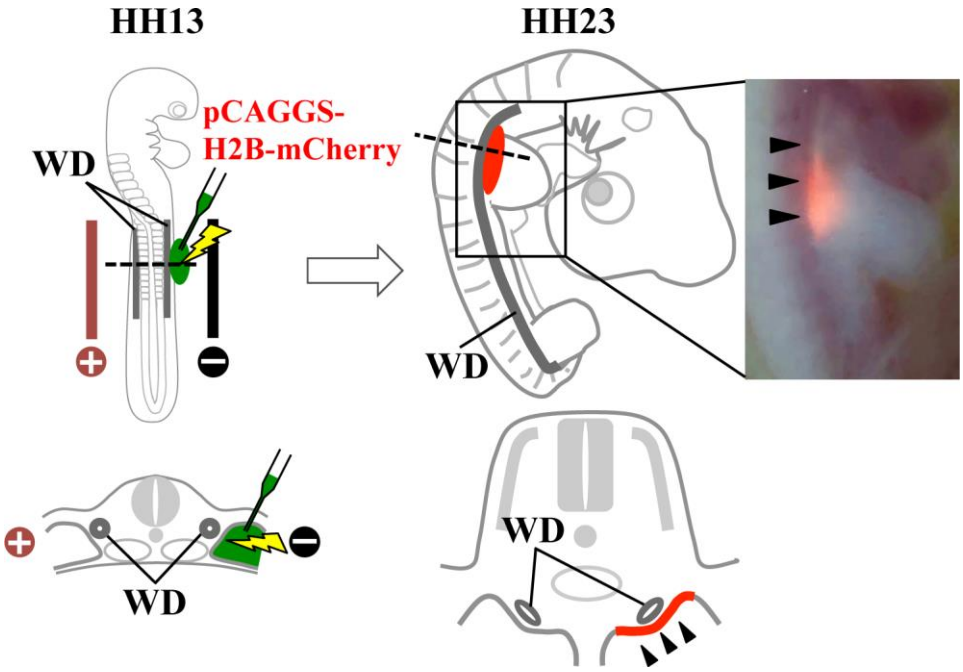

Figure S2

Diagrams illustrating procedures of in ovo electroporation into MFR. A DNA solution (pCAGGS-H2B-mCherry) shown in green was injected into the coelomic cavity of HH13 embryos. Horizontally positioned electrodes are indicated as + (anode, red) and – (cathode, black). The photo shows mCherry signals seen in presumptive MD of an HH23 embryo (arrowheads).

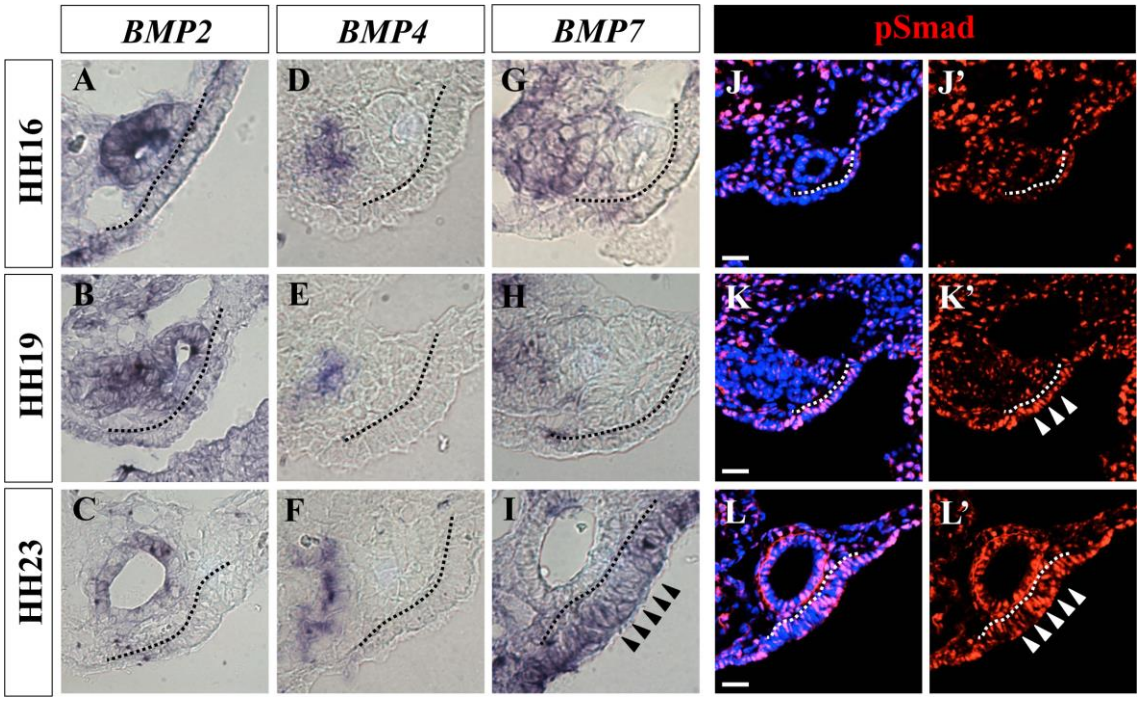

Figure S3

Expression patterns of BMP2/4/7 in the mesonephric region, and activation of Smad1/5/8 in MFR. (A-I) *In situ* hybridization to show expression of *BMP2* (A-C), *BMP4* (D-F) and *BMP7* (G-I) in HH16, HH19 and HH23 embryos. Arrowheads in I indicate *BMP7* expression in MFR. (J-L) Immunostaining for phosphorylated Smad1/5/8 (pSmad). Signals for pSmad were detected at HH19 and HH23 (white arrowheads in K', L'). Scale bars: 20 μm in J, K, L.

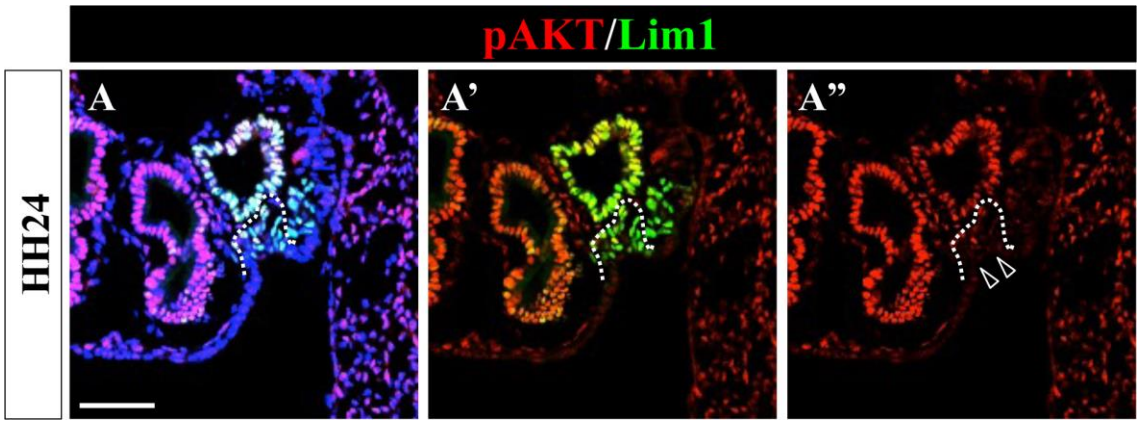

Figure S4

Immunostaining against phosphorylated AKT (pAKT). (A) Open arrowheads in A" show no signal of pAKT in MD precursors at HH24. Scale bar: 100 μm.

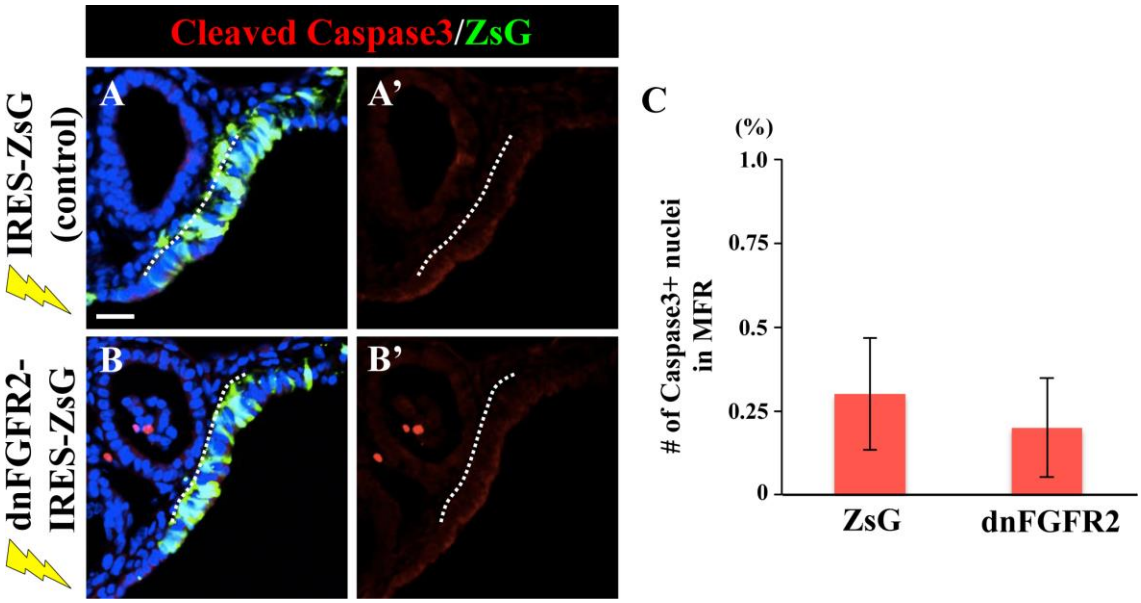

Figure S5

Inhibition of FGF signaling did not affect cell survival. (A, B) Transverse sections of ZsG- (control; A) or dnFGFR2-electroporated HH23 embryos (B) were stained with antibodies for cleaved Caspase3 (red) to visualize apoptotic cells. (C) Quantification of apoptotic cells within ZsG- or dnFGFR2-electroporated MFRs (n = 10 each). Inhibition of FGF signaling by dnFGFR2 did not excessively induce cell deaths. Error bars represent SEM. Scale bar: 20 μm in A.

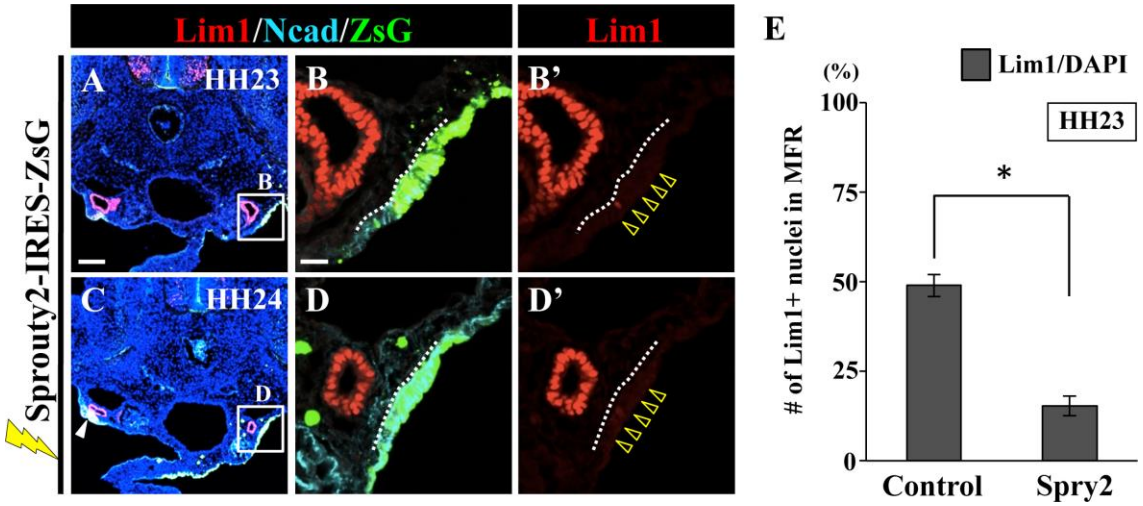

Figure S6

Misexpression of Sprouty abrogated the specification and invagination of MD precursors. (A-D) Sections of HH23 and HH24 embryos electroporated with *Sprouty2* cDNA (n = 12 for each stage). Signals for Lim1 (red) were not detected in the electroporated MFRs as indicated by yellow open arrowheads. (E) Quantitative representation of the number of Lim1-positive cells in ZsG-electroporated- and Sprouty2-electroporated MFR in HH23 embryos. Error bars represent SEM. *$p < 0.01$. Scale bars: 100 μm in A; 20 μm in B.

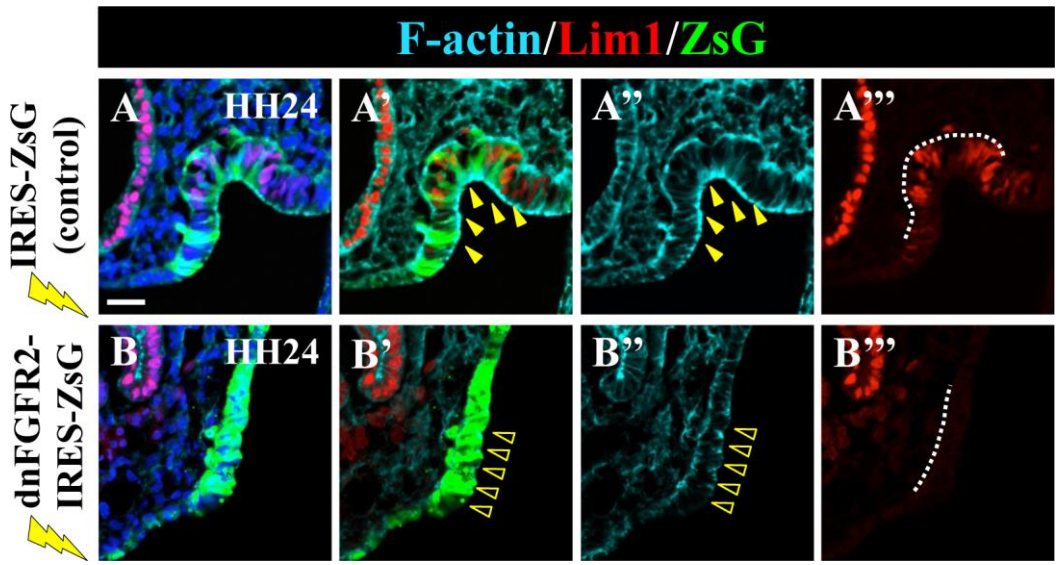

Figure S7

F-actin organization of MFR was controlled by FGF signaling. (A-B) F-actin (cyan) was depleted in dnFGFR2-electroporated MFR of HH24 embryo (open arrowheads in B; n = 8). Scale bar: 20 μm in A.

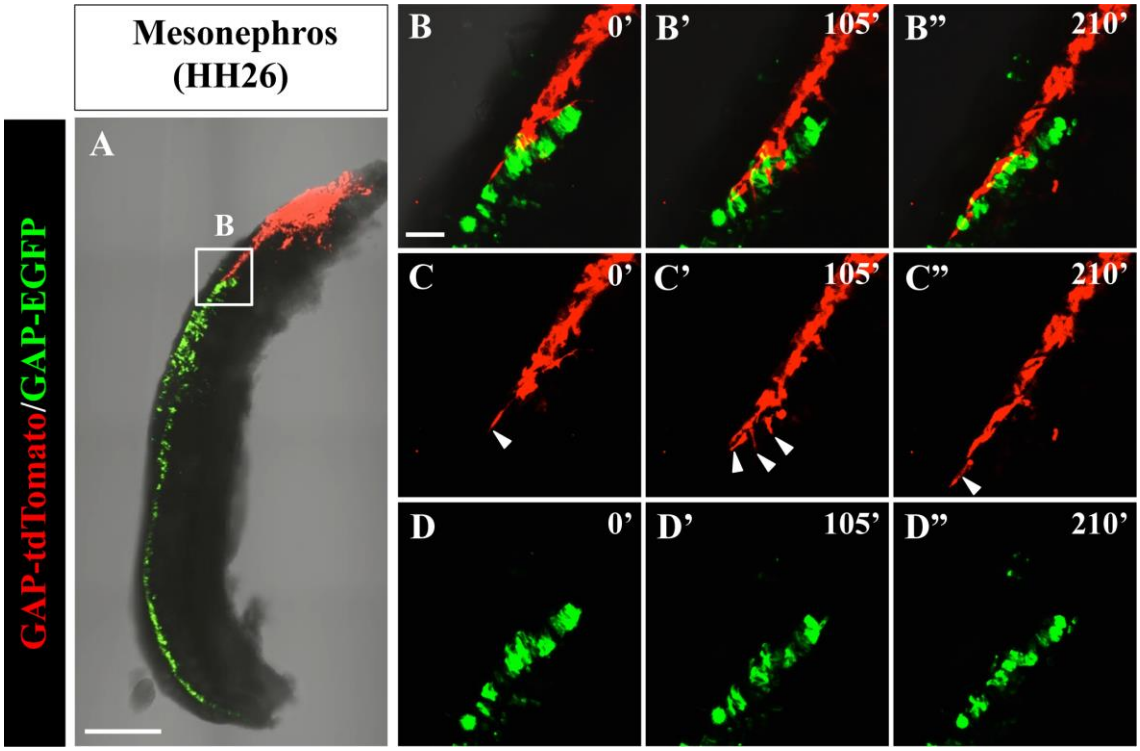

Figure S8

Time-lapse images of elongating MD. (A) A mesonephros explant from HH26 embryo was cultured *in vitro*, and imaged for 210 min. (B-D) Selected frames from the time-lapse movie (Movie S1) showing that GAP43-tdTomato-electroporated MD cells (red) migrated along GAP43-EGFP-electroporated WD (green). Pseudopodia were observed on leader cells of MD as indicated by white arrowheads in (C). Scale bars: 500 μm in A; 50μm in B.

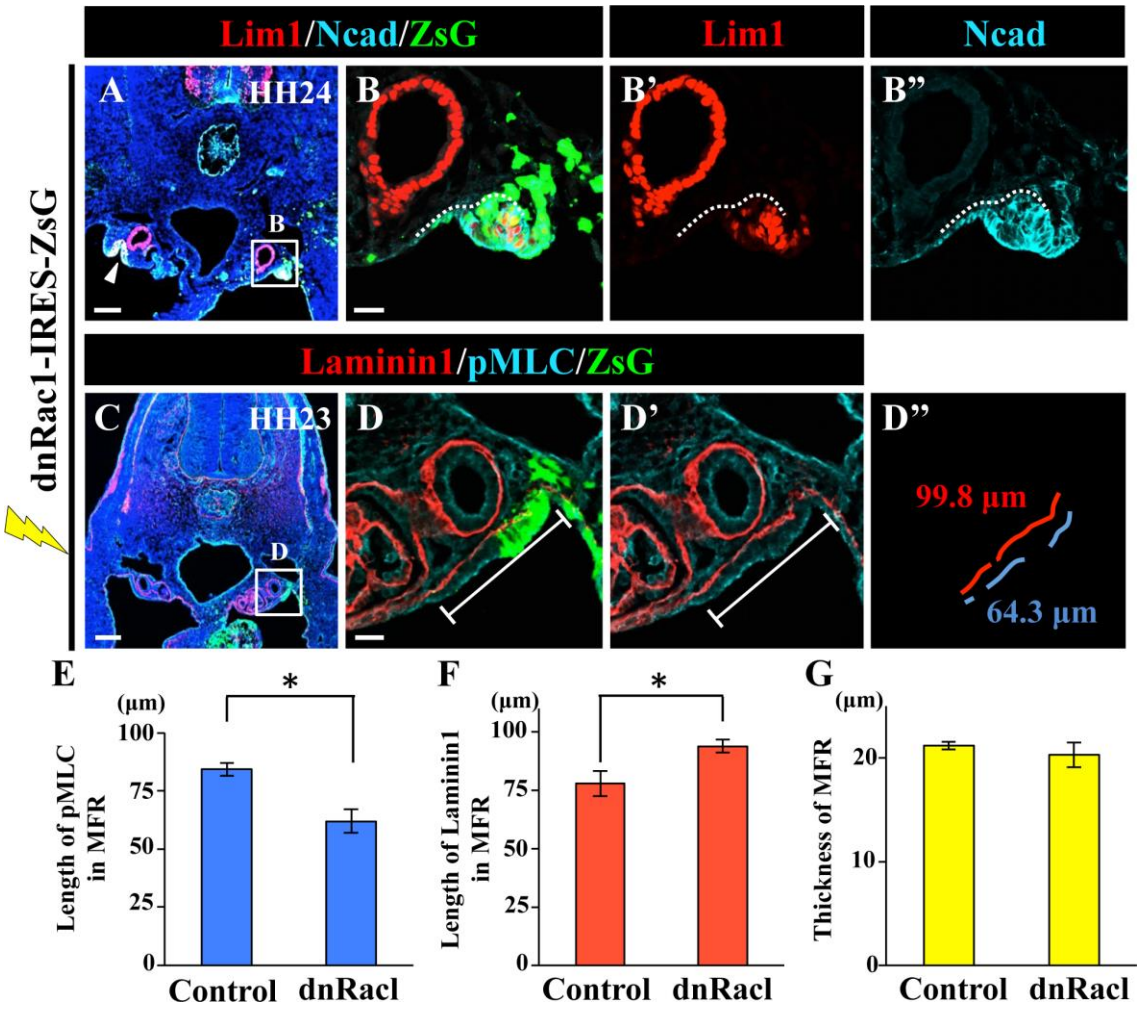

Figure S9

Implication of Rac1 in MD invagination. (A, B) A dominant negative form of Rac1 (dnRac1) electroporation caused a failure of MD invagination (n = 15). Note that misexpression of dnRac1 did not significantly affect Lim1 expression in MD precursors. (E-G) Graphs showing pMLC-length (E), Lamin1-length (F) and thickness (G) of IRES-ZsG- and dnRac1-IRES-ZsG electroporated MFRs (n = 10 each). Error bars represent SEM. *$p < 0.05$. Scale bars: 100 µm in A, C; 20 µm in B, D.

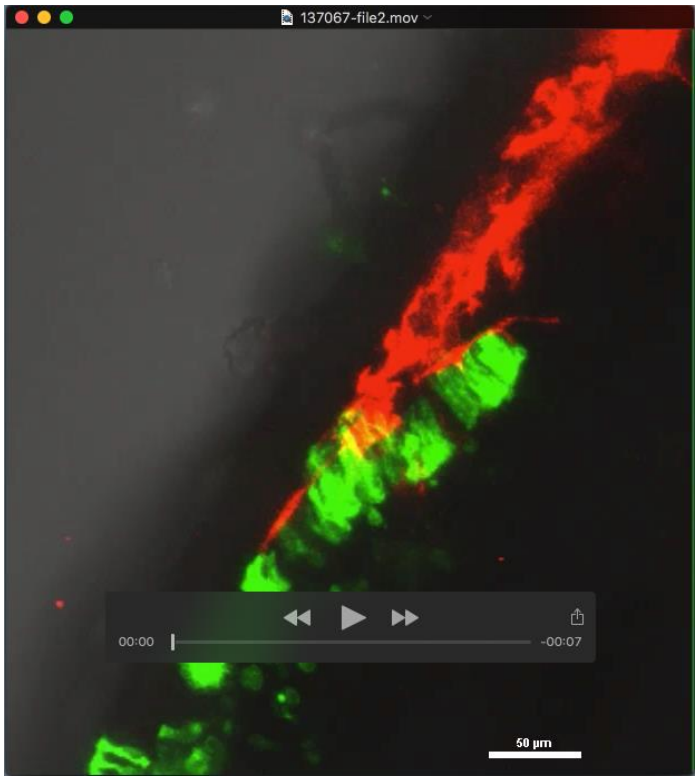

Movie S1

Time-lapse analyses using a cultured mesonephros where GAP-tdTomato (red) and GAP-EGFP (green) were electroporated into MD and WD, respectively. This movie corresponds to Fig. S8. Frames were taken every 3 min with a 20 x Plan-Apochromat objective lens. Total movie length: 210 min.